Research Article

# A comparative study of micro- and nano-structured di-nuclear Co(II) complex, designed to produce efficient nano-sorbent of $Co_3O_4$ applicable in the removal of $Pb^{2+}$

**Zohreh Razmara**[1]

Received: 22 October 2019 / Accepted: 16 March 2020 / Published online: 21 March 2020


**Abstract**
A di-nuclear inorganic complex, formulated as $[Co_2(H_2O)_5(pdc)_2]\cdot 2H_2O$ (**1**) that $pdc^{2-}$ is pyridine-2,6-dicarboxylato has been synthesized under hydrothermal condition and sonochemical irradiation. Depending on the synthetic conditions, different morphology has been obtained for complex **1**. Complex **1** hydrothermal (**hc**) which obtained as single crystal is a micro-structured compound and was characterized by single crystal X-ray diffraction. Complex **1** ultrasound (**uc**) is a nano-structured compound and obtained as precipitate. Structural comparison of **hc** and **uc** by Fourier-transform infrared spectroscopy (FT-IR), powder X-ray diffraction, and scanning electron microscopy (SEM) revealed that both synthesized complexes have the same structure with different particles size and morphology. In this study, a new synthetic route has been developed to prepare $Co_3O_4$ nanoparticles for environmental catalytic applications. Effective sorbents $Co_3O_4$-**hc** and $Co_3O_4$-**uc** were prepared by thermolysis of dinuclear cobalt complexes and characterized by FT-IR, SEM, XRD, and Brunauer–Emmett–Teller specific surface area. $Co_3O_4$-**hc** and $Co_3O_4$-**uc** were used as nano-sorbents for the removal Pb(II) from aqueous solution. Detailed sorption studies showed that both synthetic sorbents are valuable to remove Pb(II) from wastewater. The effective catalytic performance of the as-prepared sorbents can be attributed to the physicochemical features of synthetic catalysts, such as mesoporous nature, homogenous dispersion of the active phase, small particle size and high surface area. The effects of contact time, pH, Pb(II) and adsorbent dosage to remove Pb(II) were investigated. Maximum adsorption percent of $Co_3O_4$-**hc** and $Co_3O_4$-**uc** at room temperature were found to be 90 and 92.2%, respectively. The selectivity of the as-prepared catalysts toward metal ions Pb(II), Co(II), Cr(III), Cu(II), Fe(II), Hg(II), Mn(II) and Ni(II) exhibited that $Co_3O_4$ catalysts have the highest selectivity toward Pb(II). Also, the synthetic catalysts $Co_3O_4$-**hc** and $Co_3O_4$-**uc** showed an excellent cycling performance for Pb(II) removal up to 85.3 and 83.4% recovery over five cycles.

**Keywords** Micro and nano-Co(II) complex · Hydrothermal · Sonochemistry · $Co_3O_4$ · Removal of $Pb^{2+}$

## 1 Introduction

In the past few years, several reports have been presented for the preparation of nanosized metal oxides by thermolysis of inorganic complex [1–3]. For example, Zhang et al. [4] prepared nano/microparticles of $Co_3O_4$ by thermal decomposition of a metal–organic framework of cobalt-*p*-benzene dicarboxylic acid. In another study, Khalaji et al. [5] prepared $Co_3O_4$ nanoparticles with an average particles size in the range of 10–20 nm by thermal decomposition of a cobalt(III) Schiff base complex. Many methods have been attempted to prepare transition metal oxide nanoscale such as chemical vapor deposition (CVD) [6], hydrothermal methods [7], microwave irradiation [8], electrochemical deposition [9], soft chemical solution [10] and molecular beam epitaxy [11]. Several methods have been

✉ Zohreh Razmara, razmara@uoz.ac.ir; zohreh.razmara94@gmail.com | [1]Department of Chemistry, University of Zabol, P.O.Box 98613-35856, Zabol, Iran.

reported for the removal of dye and toxic metal ions from the environment such as, cloud point extraction [12], ion-exchange [13], flocculation–coagulation [14], solid-phase extraction [15], photocatalysis [16] and direct adsorption [17]. Among these methods, adsorption has been found to be the most effective with high capacity, accessibility, selectivity, simplicity of design, and separation of toxic pollutants [18]. Metal oxide nanoparticles are considered potential adsorbents in the removal of harmful heavy metals such as lead (Pb), nickel (Ni), and vanadium (V) due to their high surface area, high adsorption capacity, high chemical activity and the unique advantage of easy separation. Several reports have been published to remove heavy metal ions from contamination of water source by nano metal oxides [19–23]. For example, Uddin and Baig [24] prepared hexagonal sheet-like $Co_3O_4$ nanoparticles by a simple precipitation method. They evaluated the adsorption behavior of methyl orange onto the as-prepared $Co_3O_4$ nanoparticles. The $Co_3O_4$ NPs exhibited the remarkable adsorption properties toward methyl orange. Yavuz et al. [25] investigated the adsorption properties of Pb(II) from water, food, sediment and tobacco samples on an ultra-layered $Co_3O_4$ nanocomposite. The results of their study showed the maximum adsorption capacity of 35.5 mg/g. $Co_3O_4$ is an important transition metal oxide, with a spinel structure formulated as $AB_2O_4$ and have useful applications in catalysis, pigments, electrochromic devices, hydrocracking process of crude fuels and gas sensor [26–30]. Spinel cobalt oxide ($Co_3O_4$) is a mixed valance material that formulated as $Co^{II}Co^{III}_4$ [31] and has different morphology such as cubes, sheets, wires and tubes [32–34]. $Co_3O_4$ is found to be one of the most intriguing p-type semiconductors and better alternate materials in the separation of heavy metal ions due to its higher surface area, controllable size and shape [35]. Thermal decomposition of inorganic complexes is an effective method for the preparation of nano-catalysts which produces high activity catalysts. Previously, a number of researchers have developed many nano-catalysts from the thermal decomposition of the inorganic complexes [36, 37]. The results of their studies have shown that nanoparticles prepared by thermal decomposition of the inorganic complex have higher catalytic performance than the catalysts which prepared by other methods, such as impregnation and co-precipitation. The use of the inorganic complex as precursor for the preparation of nanoparticles potentially provides many advantages as a new route since: (a) the nanoparticles which obtained by thermolysis of inorganic complexes have high catalytic performance due to thier high surface area and small particle size [38, 39], (b) the intimate metal contact in the synthesized complexes causes their homogeneous dispersion in the catalyst structure [40]. In this study, for the first time, an effective $Co_3O_4$ nanosorbent was prepared by the thermal decomposition of a binuclear inorganic complex through the following steps. (1) A di-nuclear cobalt(II) complex formulated as $[Co(dipic)_2Co(H_2O)_5]\cdot 2H_2O$ was synthesized under different conditions. (2) The structure of the synthesized complexes were studied by single crystal X-ray diffraction (SC-XRD), FT-IR, powder X-ray diffraction (PXRD) and SEM. (3) Catalysts of $Co_3O_4$-**hc** and $Co_3O_4$-**uc** were prepared by thermolysis of hydrothermal and ultrasound complexes. (4) The synthesized catalysts were used to remove Pb(II) from aqueous solution at varied operational conditions.

## 2 Experimental

### 2.1 Reagents and apparatus

$Co(NO_3)_2\cdot 6H_2O$, pyridine 2,6-dicarboxylic acid and sodium hydroxide which used as reagents for the synthesis **hc** and **uc** complexes, were obtained from Sigma-Aldrich and used as received without further purification. Elemental analyses of carbon, hydrogen, and nitrogen were carried out using a Perkin-Elmer 2400 elemental analyzer. Infrared spectra (KBr pellets) were taken in the region of 4000–400 $cm^{-1}$ on a Jasco FT/IR-430 spectrometer. X-ray powder diffraction (XRD) measurements were performed on a Philips X-Pert MPD diffractometer (Philips electronic Co., The Netherlands) with monochromatized Cu-Kα radiation (λ = 1.54184 Å) operating at 40 kV and 30 mA with scanning rate 0.02°$s^{-1}$. The morphology and size of as-synthesized complexes and as-prepared nanoparticles were examined by scanning electron microscopy technique (SEM), using MIRA3TESCAN-XMU equipment an accelerating voltage of 15 kV. The Brunauer–Emmett–Teller (BET) surface area, pore-volume, and pore size distribution of the adsorbents were measured on PHS-1020(PHSCHINA) apparatus at 77 K from $N_2$ adsorption isotherms. In the crystallographic part, data collection was performed on a Super Nova diffractometer of Rigaku Oxford Diffraction using CuKα radiation (1.54184 Å). The crystal structure of complex **1** was solved by charge flipping using the Superflip program [40]. The refinement of the structure was performed using full-matrix least-squares on $F^2$ with the program Jana2006 [41]. The concentration of Pb(II) in the solution was determined using an inductively coupled plasma-atomic emission spectrometry, ICP-AES (PerkinElmer, Germany, 8300). Synthesis of complex **1** was carried out under ultrasounds irradiations, using a SONICA-2200 EP ultrasonic generator.

### 2.2 Synthetic strategy of complex 1 by hydrothermal method

An aqueous solution (10.0 mL) of NaOH (0.16 g, 4.0 mmol) was slowly added to an aqueous solution (40 mL) containing pyridine 2,6-dicarboxylic acid (0.33 g, 2.0 mmol) with continuous stirring at room temperature. The above-mentioned solution and an aqueous solution of $Co(NO_3)_2{\cdot}6H_2O$ (0.58 g, 2 mmol) were placed in a stainless steel vessel. The vessel was sealed and heated to 150 °C within 24 h, kept at this temperature for 4 days and then cooled to the room temperature. The resulting solution was filtered, and the filtrate was evaporated. After a few days, single crystals of **1**, suitable for X-ray analysis were collected, washed with water and dried in air. Yield: 67% based on Co. Anal. Calcd for $C_{14}H_{20}N_2O_{15}Co_2$: C, 29:28; H, 3:46; N, 4:88. Found: C, 29.32; H, 3.47; N, 4.89.

### 2.3 Synthetic strategy of complex 1 by sonochemical irradiation

In order to synthesis uc-complex by ultrasonic irradiation, an aqueous solution (10 mL) of pyridine 2,6-dicarboxylic acid (0.33 g, 2.0 mmol) which was previously deprotonated by NaOH (0.16 g, 4.0 mmol) was sonicated at about 50 °C. Into this solution, an aqueous solution of $Co(NO_3)_2{\cdot}6H_2O$ (0.58 g, 2 mmol) was added in a dropwise manner under a high-intensity ultrasonic probe operating at 20 kHz at a maximum power output of 100 W. During sonication, the temperature of the solution was controlled at about 50 °C. The obtained precipitates were filtered, washed with water and dried at 80 °C vacuum oven for 12 h. Yield: 70% based on Co. Anal. Calcd for $C_{14}H_{20}N_2O_{15}Co_2$: C, 29:28; H, 3:46; N, 4:88. Found: C, 29.32; H, 3.49; N, 4.88.

### 2.4 Thermal decomposition of synthesized complexes

Hydrothermally and sonochemically synthesized complexes were used as precursor for the preparation of $Co_3O_4$ nanoparticles using thermal decomposition. To this purpose, 10 mmol (5.7 g) of the hydrothermal complex was placed in an electric furnace at 550 °C for 6 h with a ramping rate of 10 °C/min. Similarly, annealing of **uc**-complex followed the same procedure.

### 2.5 The Pb(II) adsorption procedure

The batch adsorption experiments were performed in 250 mL Erlenmeyer flask. All adsorption experiments were conducted at room temperature under air atmosphere and the effect of pH, contact time, adsorbent and Pb(II) dosage on the uptake of Pb(II) were investigated. To perform adsorption experiments, synthetic $Co_3O_4$ as nano-sorbent was added to an aqueous solution containing Pb(II), while the pH of the solution was controlled using HCl or NaOH. The obtained suspension was placed on an orbital shaker at 200 rpm for 90 min to ensure equilibrium. At predetermined times, 2 mL of the sample was withdrawn, and centrifuged at 3600 rpm for 10 min and filtrate solutions were analyzed by ICP–AES. The pH values were adjusted by a solution of NaOH (0.1 M) or $HNO_3$ (0.1 M). The adsorption capacity ($q_e$) and adsorption percentage values for Pb(II) uptake were determined as follows:

$$\text{Removal}\,(\%) = \frac{C_o - C_e}{C_o}100 \tag{1}$$

$$q_e\,(\text{mg/g}) = \frac{C_o - C_e}{m}V \tag{2}$$

where $C_0$, $C_e$, (mg/L) are the Pb(II) concentrations at the initial and equilibrium time, respectively, V (L) is the solution volume and m (g) is the weight of used adsorbent. All the adsorption experiments were repeated three times and average values were reported. Desorption studies were performed in 5 mL of 0.1 M $HNO_3$ for 60 min. The Pb(II) adsorbed were placed in the mentioned desorbing medium on a rotary shaker at 200 rpm and followed by adsorbent separation and washed with water for several times and dried at 50 °C for 10 h. Reusability study of adsorbent catalysts was carried out by following the adsorption–desorption study for 5 cycles.

### 2.6 Effect of competing ion

The ion selectivity can be evaluated due to the co-existing of the diverse metal ion in the contaminated water. To this purpose, an aqueous solution (30 mL) containing of each Co(II), Cr(III), Cu(II), Fe(II), Hg(II), Mn(II) and Ni(II), and 1 g of sorbent was mixed. In the experimental condition, the diverse metal ions amount was 20 times higher than the Pb(II) concentration. The concentration of Pb(II) was kept constant at 10 mg/L in all experiments. The resulting suspension was stirred for 35 min at pH 5 and separated by filtration. The quantification of the elements in the solution was analyzed using ICP-AES. All the experiments were repeated two times to confirm the extracted data in this study. The highest variation for each adsorption operation was 3.2%.

## 3 Results and discussion

### 3.1 Characterization of synthesized complexes

The molecular structure of complex **1** which synthesized under hydrothermal condition and obtained as a single crystal is shown in Fig. 1. Previously, this complex was synthesized in another way [42]. Figure 2 shows a polyhedral geometry around centers of $Co^{2+}$. Two cobalt atoms have been identified in the structure of this complex. One of them is coordinated with two dipicolinate anions in the form of distorting octahedral. Each of the dipicolinate ligands is coordinated in a tridentate coordination mode. Another center of $Co^{2+}$ is surrounded by five water molecules and one μ-oxygen of carboxylate group in the form of a more ideally octahedral. A large number of inter- and intra-molecular hydrogen bonds which take place through the oxygen atoms of dipicolinate ligands, two crystalized water molecules and five coordinated water molecules are found in the structure of this complex. A huge three-dimensional network is created by these hydrogen bonds that stabilize the crystalline structure of the complex (Fig. 3).

Figure 4, shows the simulated XRD powder pattern of complex **1** which obtained of **uc** (Fig. 4a), **hc** (Fig. 4b) and crystallographic data (Fig. 4c). It can be clearly seen that there is an acceptable match between these patterns. This confirms that the structure of complex **1** which synthesized by the hydrothermal method is the same to that synthesized by the sonochemical process. All three patterns contain diffraction peaks at $2\theta = 6.5°$, 9.8°, 11.1°, 14.6°, 16.5°, 18.6°, 23.1°, 24.7°, 27. 2° 30.6° and 42.5° which are attributed to the pure phase of $[Co_2(H_2O)_5(pdc)_2]\cdot 2H_2O$. Complex 1 crystalizes in a monoclinic system with space group = P $2_1/c$ and the lattice parameters a = 8.3906(3) Å, b = 27.4005(8) Å, c = 9.6192(4) Å that are very close to the reported data (CCDC = 208,426) [42]. Figure 5, shows the FT-IR spectra of **hc** and **uc** complexes. As the figure shows, these two spectra are in perfect agreement with each other and the complexes appear to have the same structure. As shown in Fig. 5, broadband at 3200–3600 $cm^{-1}$ is assigned to the stretching vibration of OH groups, belongs to adsorbed, crystallized and coordinated water molecules. The characteristic and strong band of the asymmetric vibration of carboxylate groups is appear at 1630 $cm^{-1}$ which this peak overlaps with the bending modes of adsorbed and

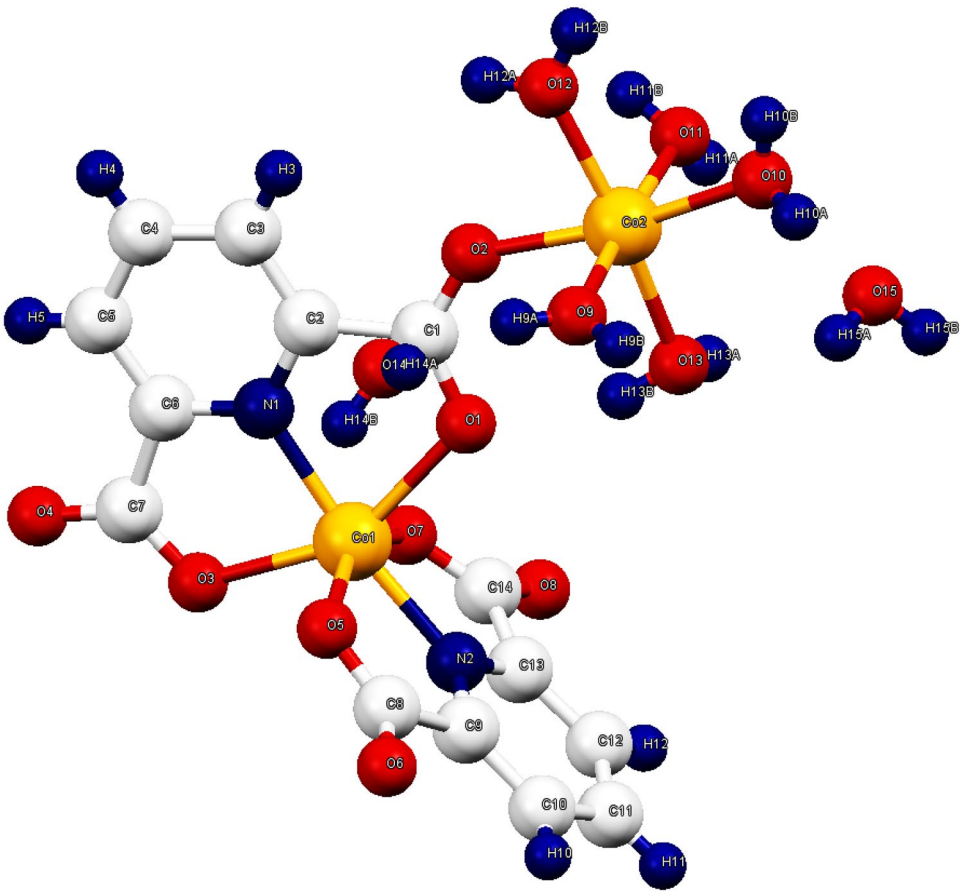


**Fig. 1** Molecular structure of complex **1**

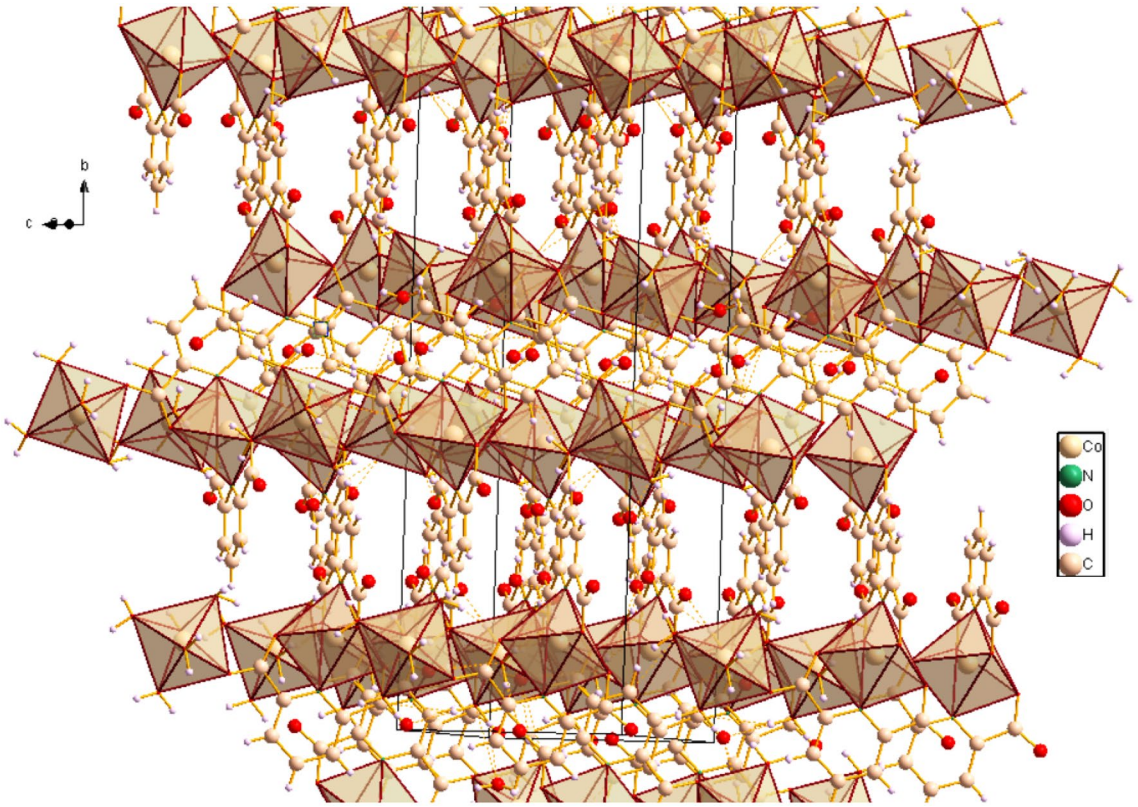


**Fig. 2** A polyhedral geometry around centers of $Co^{2+}$ in complex **1**

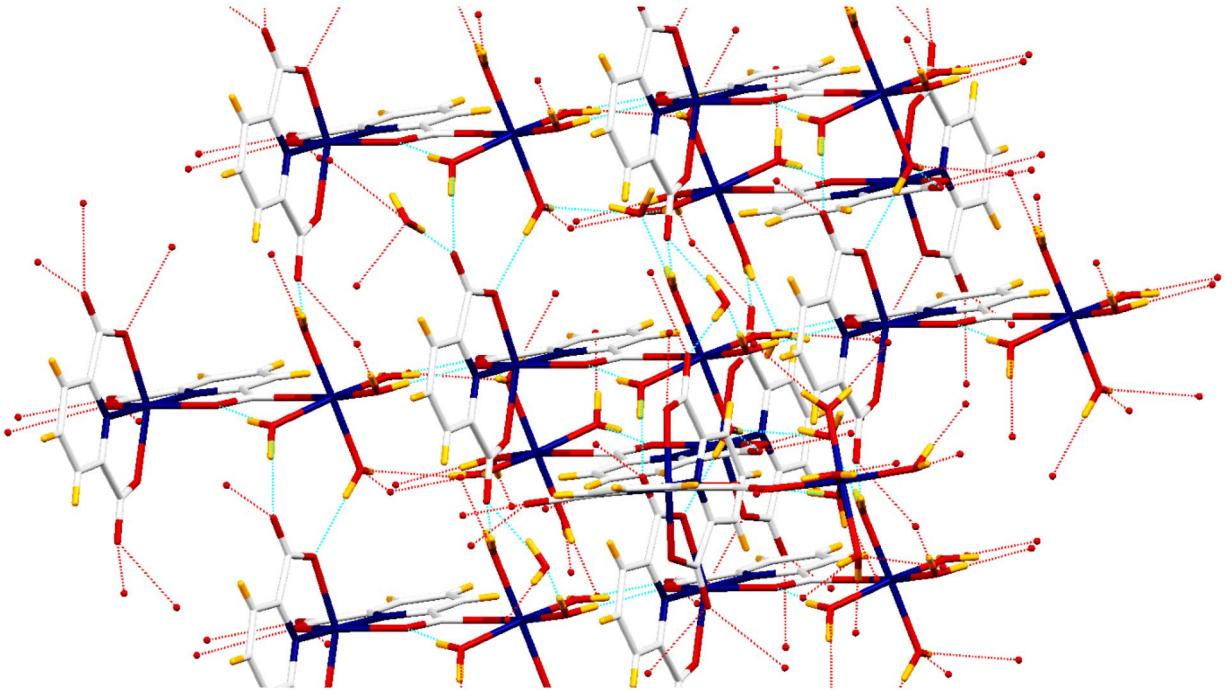

**Fig. 3** A part of the 3D network created by the intra- and inter-molecular hydrogen bonds of complex **1**

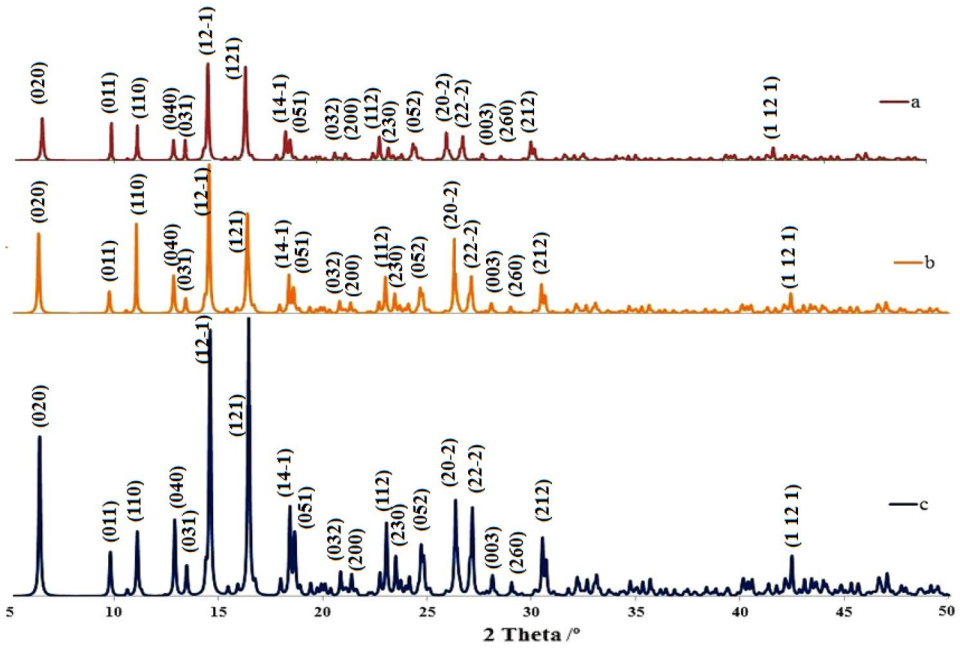


**Fig. 4** XRD patterns of **a** ultrasound complex, **b** hydrothermal complex, **c** based on single crystal data of hydrothermal complex

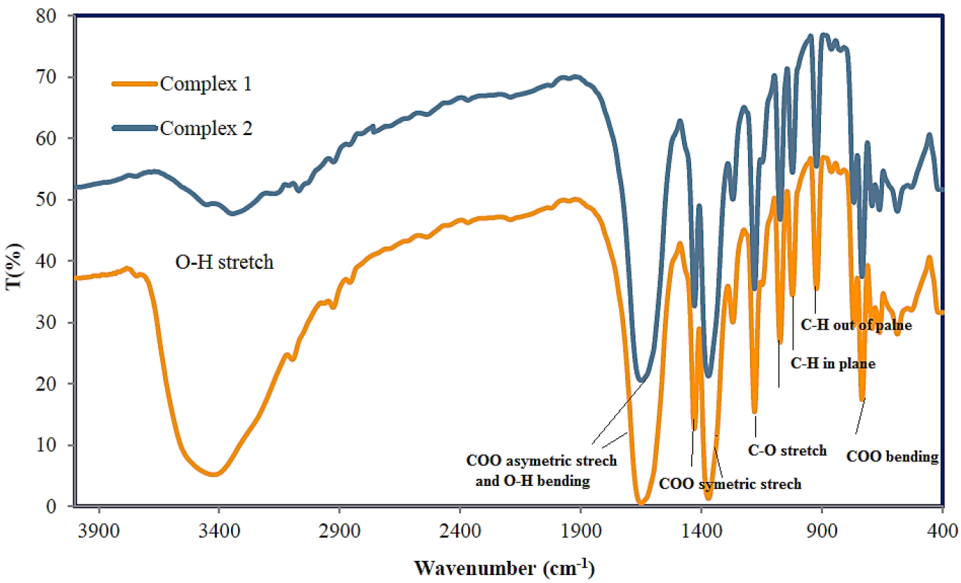


**Fig. 5** The FT-IR spectra of complex 1 (**uc**) and complex 2 (**hc**)

coordinated water molecules [43, 44]. The peaks in 1429 and 1378 $cm^{-1}$ are due to the symmetric vibration of carboxylate groups. Frequency difference between the asymmetric and symmetric vibrations modes of carboxylate groups is 201 $cm^{-1}$, which is corresponding to the mono-dentate interaction between the $COO^-$ of carboxylate groups and the Co atom of synthesized complexes [45, 46]. The peak corresponding to the stretching vibration band of C–O can be seen at 1183 $cm^{-1}$. The frequencies at 1080 and 918 $cm^{-1}$ is attributable to C–H in-plane and out-of-plane bending modes, respectively [47, 48]. Also, the peak at 761 $cm^{-1}$ is due to the bending mode of δ(O–C–O) [49, 50]. The bands at 660 and 585 $cm^{-1}$ are due to the stretching vibration modes of Co–N and Co–O, respectively. In order to obtain further information and the role of synthetic method on the morphology and particles size of as-synthesized complexes, SEM micrographs of **uc** and **hc** complexes were investigated (Fig. 6). As seen in Fig. 6a, the morphology of the synthesized complex via hydrothermal method is irregular which its diameter was found to be around 0.42 µm. Whereas, the average particles size of the synthesized complex via the sonochemical process was found to be around 56.4 nm. It seems that the generated ultrasound and high power irradiation prevent the particles growth and keep the particles formed in small size. Previously,

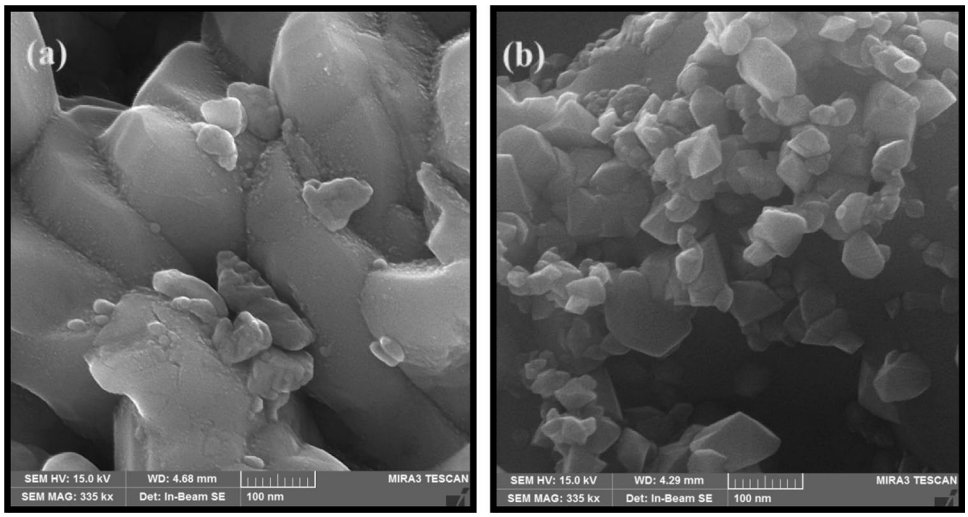


**Fig. 6** SEM photographs of **a** hc and **b** uc

many nanostructure compounds with various morphologies have been synthesized by ultrasonic irradiation. For example, Pugazhenthiran and co-workers prepared Au–$Bi_2O_3$/$Bi_2O_3$ nanocatalysts via sonochemical method [51]. In another study, Hayati and his colleagues synthesized nano supramolecular compounds of two new 1D and 0D, mercury(II) by a sonochemical process [52]. The results of their study showed that temperature, sonication power and time of irradiation had a very significant effect on the particles size of synthesized complexes.

### 3.2 Characterization of $Co_3O_4$-hc and $Co_3O_4$-uc

Figure 7 shows the FT-IR spectra of $Co_3O_4$-**hc** and $Co_3O_4$-**uc** which prepared by thermal decomposition of **hc** and **uc** complexes, respectively. It is clearly seen that both prepared catalysts have the similar spectrum. In the spectrum of as-prepared samples, the broad absorption band at 3200–3600 $cm^{-1}$ is attributed to the stretching vibration of hydroxyl groups of adsorbed water molecules on the surface of the nanoparticles. The tiny peak observed at 1620 $cm^{-1}$ in the spectrum of $Co_3O_4$-**uc** can be attributed to the bending mode of adsorbed water molecules. It is also found that the spinel structure of $Co_3O_4$ shows two absorption bands at 680 and 560 $cm^{-1}$ which can be assigned to the stretching vibration band of $Co^{2+}$-O with tetrahedral coordination mode and $Co^{3+}$-O bond with octahedral coordination mode, respectively [51]. Figure 8 shows the XRD powder patterns of $Co_3O_4$-**hc** and $Co_3O_4$-**uc**. The figures confirmed that the patterns completely consistent with the standard patterns of spinel $Co_3O_4$ with JCPDS card No. 74–1656. It can be seen that all diffraction peaks with intensities of (220), (311), (222), (400), (422), (511), (440), (533) are perfectly indexed to the pure cubic phase of $Co_3O_4$ with the lattice parameters a = 8.0840 Å and S.G = Fm-3 m [53, 54]. The Debye–Scherrer equation has been used to estimate the crystallite size of synthesized sorbents. The main limitation in the

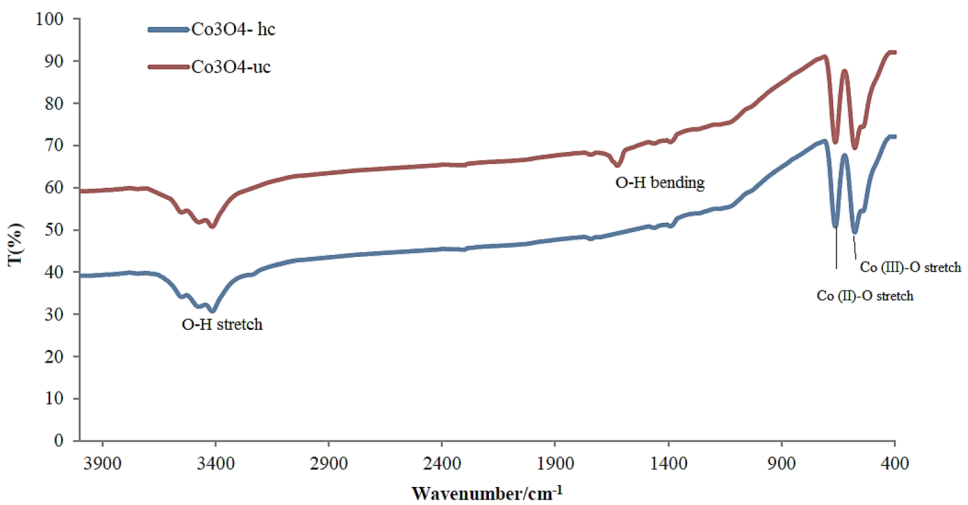


**Fig. 7** The FT-IR spectra of $Co_3O_4$-**hc** and $Co_3O_4$-**uc**

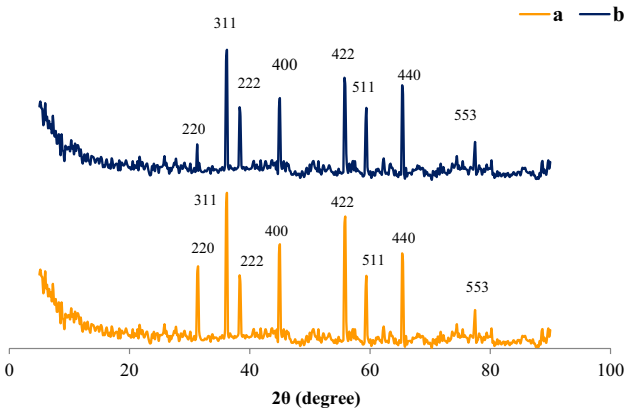


**Fig. 8** XRPD patterns: (a) $Co_3O_4$-**uc**, (b) $Co_3O_4$-**hc**. The peaks are indexed according to the cubic $Co_3O_4$ (JCPDS No. 74–1656)

application of the Scherrer equation concerns the type of studied materials, which is restricted to determining the size of the crystallite and does not include amorphous materials. Both synthetic sorbents $Co_3O_4$-**hc** and $Co_3O_4$-**uc** have an average crystallites size of 41 nm, 38.5 nm, respectively which estimated using the Scherrer's equation, $D = k \cdot \lambda / \beta 1/2 \cdot \cos(\theta)$ [55, 56], where D is the mean crystalline diameter (nm), k is a constant equal to 0.9, λ is the X-ray radiation wavelength, β1/2 is the full width half maximum (FWHM) of the sample diffraction peaks and θ is the Bragg diffraction angle. Surface morphological and detailed information of $Co_3O_4$-**hc** and $Co_3O_4$-**uc** were investigated using SEM (Fig. 9). It can be clearly found that $Co_3O_4$-**hc** and $Co_3O_4$-**uc** are nanometer-scale with an average particles size of 43 nm and 40 nm, respectively. Furthermore, it can be seen that the $Co_3O_4$-**hc** and $Co_3O_4$-**uc** consists of randomly aggregated with irregular morphology. The textural characterization and surface properties of as-prepared $Co_3O_4$-**hc** and $Co_3O_4$-**uc** nanoparticles were investigated using $N_2$ sorption analysis (Fig. 10). Figure 10a shows the adsorption–desorption isotherms and Fig. 10b shows the BJH pore size distribution plots of as-prepared samples. As shown in Fig. 10a, both synthetic $Co_3O_4$-**hc** and $Co_3O_4$-**uc** belongs to type IV-like profiles with slight hysteresis loops at relatively high relative pressure and characterized as mesopores materials which confirm the porosity of the nanoparticles' surfaces and show the high ability of adsorption [57, 58]. The specific surface areas which were calculated by Brunauer–Emmett–Teller (BET) method for $Co_3O_4$-**hc** and $Co_3O_4$-**uc** were found to be 75.7 and 82 $m^2/g$, respectively. As shown in Fig. 10b, the as-prepared samples displayed a relatively concentrated pore distribution calculated with BJH method ranging from 0.2 to 7 nm. Also, the pore volume is estimated to be 0.77 $m^3/g$ and 0.81 $m^3/g$ for $Co_3O_4$ -**hc** and $Co_3O_4$ -**uc**, respectively.

## 3.3 Studies of sorption

### 3.3.1 Effect of pH

The adsorption of Pb(II) on the surface of $Co_3O_4$-**hc** and $Co_3O_4$-**uc** is found to be pH-dependent because of its effect on the active sites and the structure of nano-adsorbents. In order to examine the effect of pH on the adsorption of Pb(II), the pH values of solution were changed in the pH range of 2–9 (Fig. 11) by using an initial Pb(II) concentration of 10 mg/L at shaking time and shaking rate of 50 min and 200 rpm, respectively. As shown in Fig. 11, the percentage of removed Pb(II) by $Co_3O_4$-**hc** and $Co_3O_4$-**uc**, increases with increasing pH until pH 5, when it reaches the maximum value of 83% and 87.4%, respectively. Below pH 5, the amount of adsorption of Pb(II) on the catalyst surface is lower, because the surface of the catalyst has a positive charge and repels Pb(II) [59–61]. Yavuz et al. [62] showed that the decrease in removal Pb(II) at low pH, can

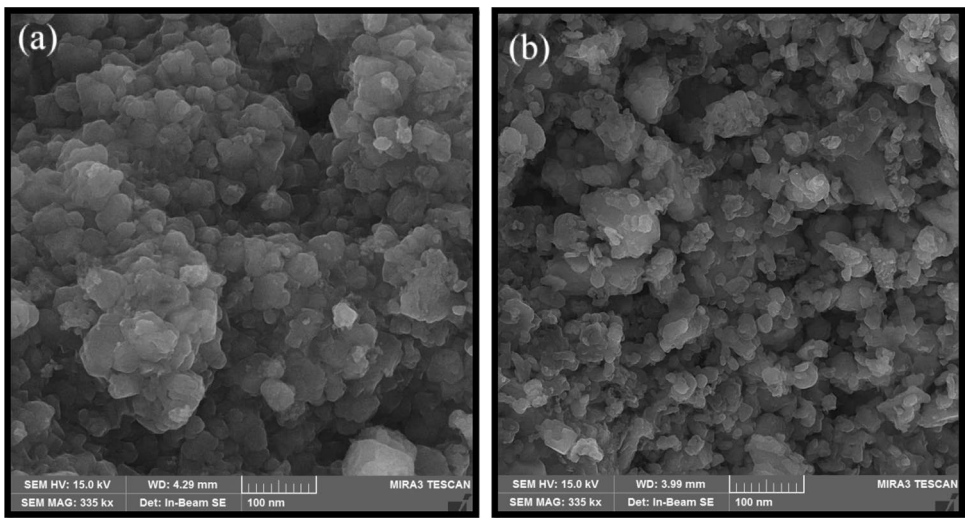


**Fig. 9** SEM micrographs of **a** $Co_3O_4$-**hc** and **b** $Co_3O_4$-**uc**

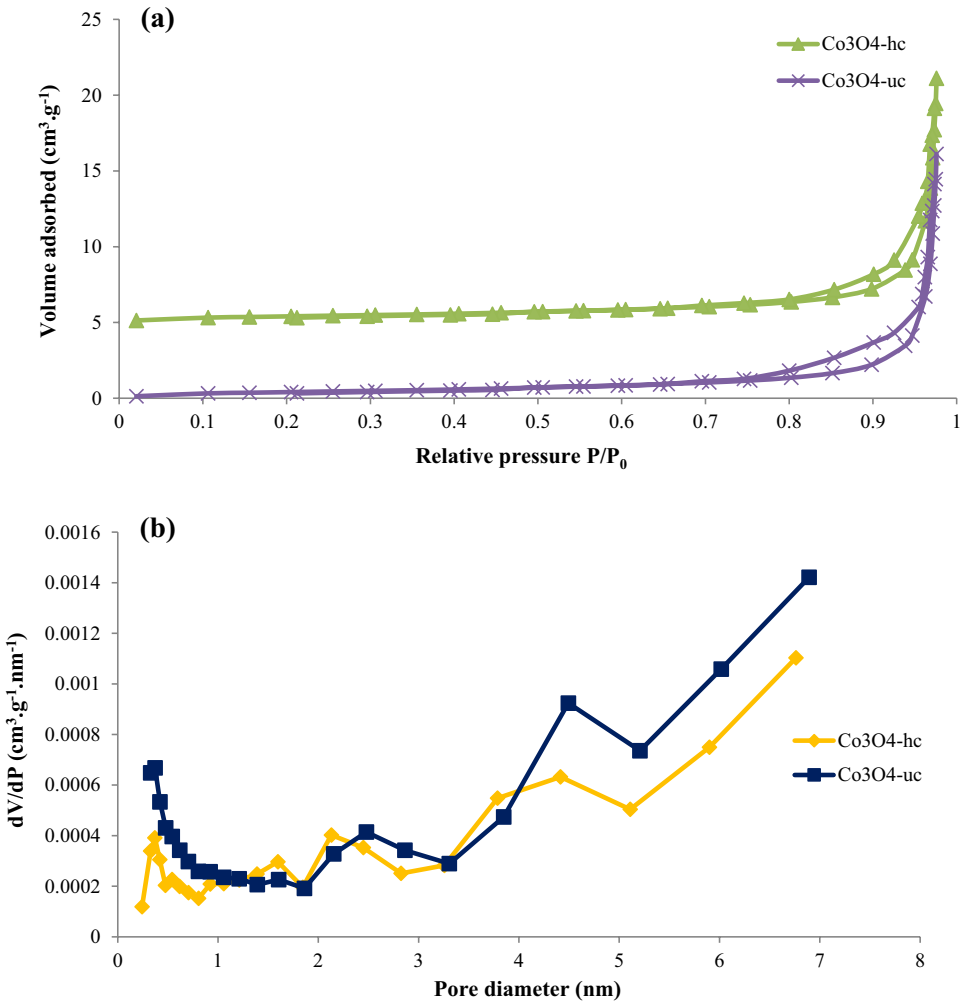


**Fig. 10** **a** Nitrogen adsorption/desorption isotherm of $Co_3O_4$-**hc** and $Co_3O_4$-**uc** and **b** BJH pore size distribution of $Co_3O_4$-**hc** and $Co_3O_4$-**uc**

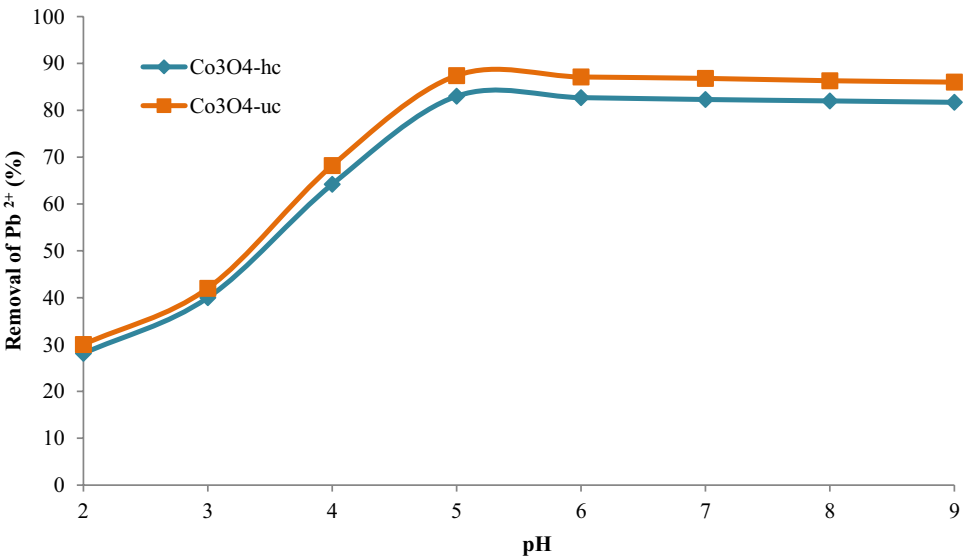


**Fig. 11** The effect of pH on the adsorption of $Pb^{2+}$ onto $Co_3O_4$-hc and $Co_3O_4$-uc adsorbent dosage = 0.1 g/L, contact time = 50 min at concentration 10 mg/L of $Pb^{2+}$

be attributed to the competition of $H^+$ and $Pb^{2+}$ions for the adsorption on the active sites of $Co_3O_4$. In the second region (pH 6.0–9.0), the removal of Pb(II) was almost constant and nearly maintains the maximum value. When the pH reaches above 9.0, the removal of Pb(II) is possible to accomplish by the precipitation of Pb(II) as hydroxides and simultaneous adsorption [63].

### 3.3.2 Effect of contact time

The experimental results of the effect of contact time on the adsorption of Pb(II) onto $Co_3O_4$-**uc** are shown in Fig. 12. To achieve this, the adsorption changes of a model solution containing 10 mg/L of Pb(II) at pH 5 was studied at different contact times changing from 10 to 50 min. The adsorption of Pb(II) increases with increasing contact time and reaches the maximum value of 92.2% at 35 min. It can be seen that the removal of Pb(II) is rapid at the initial stage, while it gradually slows down until it reaches equilibrium. The initial rapid increase in the adsorption rate is attributed to the availability of more adsorption sites. After 35 min, adsorption decreases with the increase in contact time that this may be due to desorption process [64, 65].

### 3.3.3 Effect of adsorbent dosage

Figure 13 shows the effect of sorbent type and its dosage on the removal of Pb(II) while all other experimental conditions are kept constant at optimum conditions. The results show that the capacity of an adsorbent is highly dependent on the sorbent dosage. As shown in the figure, when the adsorbent concentration increased to 0.1 g/L, the adsorption percent on the surface of $Co_3O_4$-**uc** and $Co_3O_4$-**hc** increased to, 92.2 and 90%, respectively. It has been observed that with increasing catalyst concentration the number of active sites increases, resulting in an increase in the rate of Pb(II) removal. It is observed that after a dosage of 0. 1 g/L, with increasing adsorbent dose, a decrease in Pb(II) adsorption was observed. It may be due to the saturation of sorption sites through the sorption

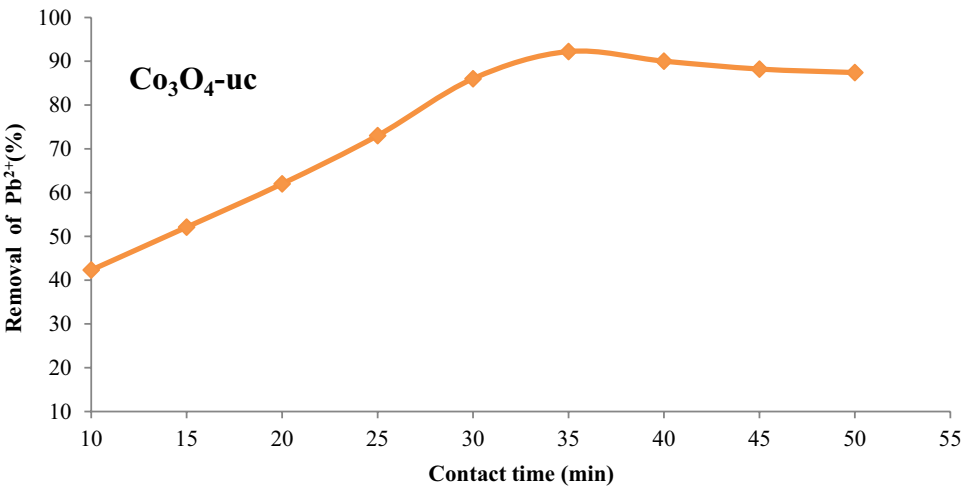


**Fig. 12** Effect of contact time on the adsorption of Pb(II) onto $Co_3O_4$-uc at pH 5

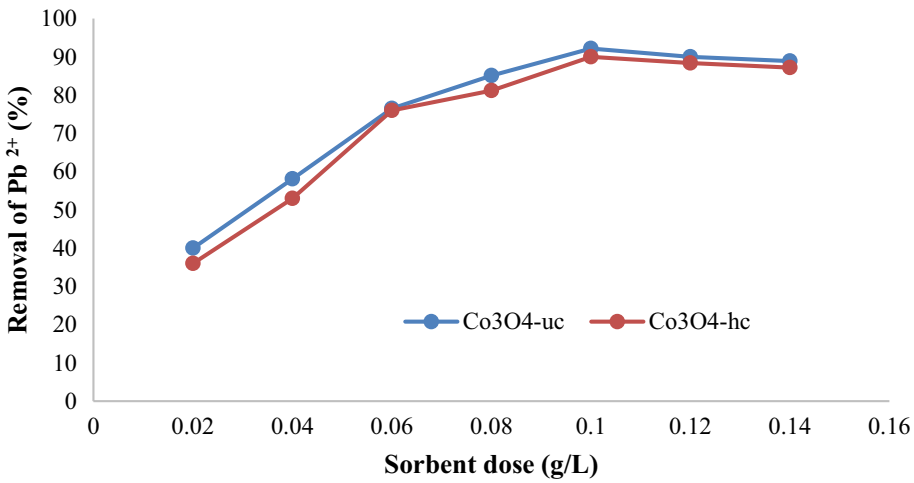


**Fig. 13** Effect of sorbent dose and sorbent type on the removal of $Pb^{2+}$

process and aggregation resulting from high sorbent dose [66]. The high performance exhibited by synthetic catalysts is attributed to increase in the specific surface area of sorbents and the availability of more active sites [67], which could be a result of the method of preparation. The preparation method plays an important role in the performance and activity of the catalysts, because it can affect the physicochemical properties of the catalysts. As mentioned in the previous section, the preparation of $Co_3O_4$-**uc** and $Co_3O_4$-**hc** through thermolysis of dinuclear inorganic complex lead to creating some features such as high active phase dispersion, small particle size and high specific surface area [38, 39]. However, adsorption efficiency can be affected by several parameters such as particles size, BET surface area, and crystalline phase. A higher specific surface area and smaller particle size of sorbent can increase the number of metal ions adsorbed on the sorbent surface. As mentioned in the previous section, the specific surface area of $Co_3O_4$-**uc** is only slightly higher (8 $m^2$/g) than of $Co_3O_4$-**hc** and this is likely related to the particles size of the sorbents. It has been shown that, although the precursors of **uc** and **hc** used for the preparation of two adsorbents have the different specific surface area and the particles size, after thermal decomposition of inorganic precursors at the same temperature and time, the specific surface area and particle size of as-obtained sorbents is close to each other. Previously, many sorbents have been prepared to remove $Pb^{2+}$ from water sources. For example, Khan et al. [68] prepared $Co_3O_4$ co-doped $TiO_2$ nanoparticles by thermal decomposition method at low temperature with applicable in the adsorption of Pb(II) from aqueous solution. They showed that this nanocomposite has the high selectivity toward Pb(II) with uptake capacity of 114.05 mg/g. Table 1 shows the maximum adsorption capacity of $Pb^{2+}$ by different adsorbents.

**Table 1** Comparative data on various adsorbents for Pb(II) reported in literature

| Adsorbent | Maximum adsorption capacity (mg/g) | References |
|---|---|---|
| $Co_3O_4$ co-doped $TiO_2$ | 114.05 | [68] |
| Xanthate-modified magnetic chitosan (XMCS) | 76.9 | [69] |
| Neem leaf powder | 300 | [70] |
| $SiO_2$/graphene composite | 113.6 | [71] |
| Functionalized graphene ($GNS^{PF6}$) | 406.6 | [72] |
| EDTA-graphene oxide | 497 ± 46 | [73] |
| $Co_3O_4$-**hc** and $Co_3O_4$-**uc** | 135 and 138.3 mg/g, respectively | In this study |

### 3.3.4 Effect of Pb(II) concentration

In order to investigate the effect of Pb(II) concentration on the adsorption rate, variable concentrations of Pb(II) from 4 to 14 mg/L were selected under the optimized conditions, contact time 35 min, pH 5 and adsorbent dose (0.1 g/L). All experiments were carried out at room temperature. As shown in Fig. 14, as Pb(II) concentration increased from 4 to 12 mg/L, the adsorption of Pb(II) on the surface of $Co_3O_4$-**hc** and $Co_3O_4$-**uc** were enhanced to 94.4 and 96%, respectively. This is probably because as the concentration of Pb(II) increases, the diffusion of Pb(II) onto sorbent is facilitated due to the increase in the driving force of the concentration gradient [74]. It means that at initial concentrations of Pb(II), the mass transfer between sorbent and Pb(II) solution and availability of unoccupied binding sites is high. However, Dye removal efficiency decreased to less than 85 and 84.3% on the surface of $Co_3O_4$-**uc** and $Co_3O_4$-**hc**, respectively, at concentrations of 14 mg/L of Pb(II), because of nearly complete coverage the binding sites at high Pb(II) concentration.

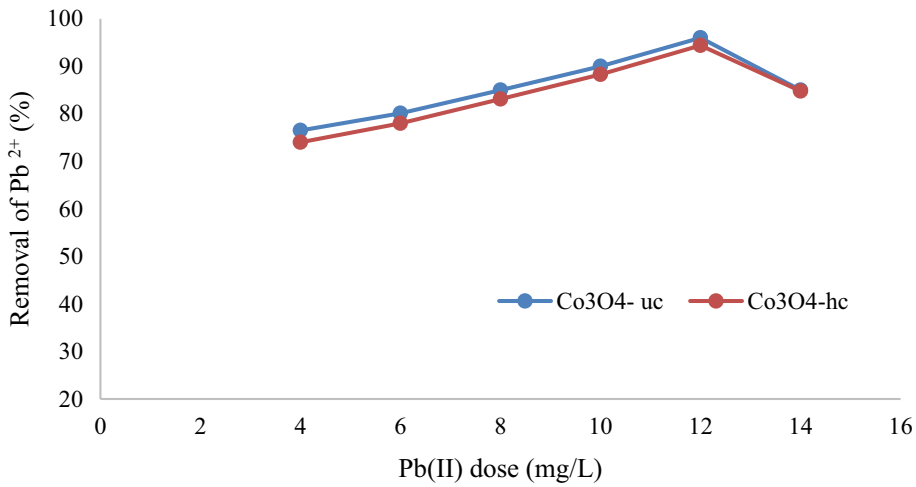


**Fig. 14** Effect of Pb(II) dose on the removal of $Pb^{2+}$

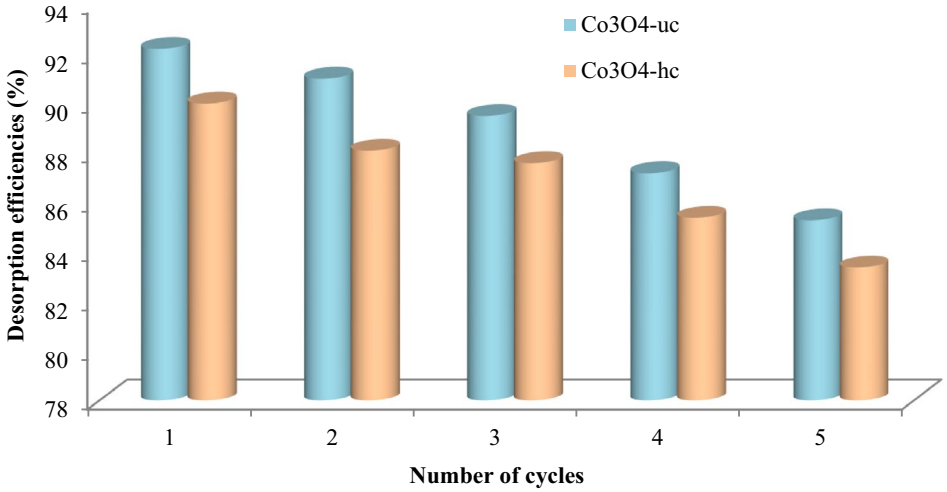


**Fig. 15** Recovery (%) of $Co_3O_4$-hc and $Co_3O_4$-uc

### 3.3.5 Selectivity study of $Co_3O_4$ nanoparticles

The contaminated water is containing several metal ions along with the Pb(II) ion which competes with each other for available adsorption sites and may affect Pb(II) selectivity [75, 76]. The Pb(II) adsorption percentage of synthesized catalysts was studied in the presence of diverse metal ions. The results obtained from the selectivity study showed that the synthetic catalysts of $Co_3O_4$-**hc** and $Co_3O_4$-**uc** have the highest selectivity toward Pb(II). The uptake of Pb(II) ion on the $Co_3O_4$-**uc** and $Co_3O_4$-**hc** catalysts is as high as 86 and 82.4%, respectively. While other ions showed much lower amounts of adsorption. However, the highest amount of adsorption was observed by Cr(III) (23%).

### 3.3.6 Desorption and reusability of the adsorbent

The stability and potential regeneration of an adsorbent are the very important feature for repeated use, industrial applications and in economic points of view. To investigate the reusability of $Co_3O_4$-**hc** and $Co_3O_4$-**uc**, five adsorption–desorption cycles were repeated under the batch experimental conditions. Desorption of Pb(II) from the adsorbent has been performed by $HNO_3$ (2 mol/L) and ultra-high purity water, respectively. The resulting mixture was shaken for 60 min to reach desorption equilibrium and finally the nano-sorbent was collected using centrifugation. As shown in the Fig. 15, after five cycles, approximately 85.3 and 83.4% of Pb(II) adsorbed on the surface of $Co_3O_4$-**uc** and $Co_3O_4$-**hc** was desorbed that demonstrates good stability and reusability for adsorbents.

## 4 Conclusion

In this paper, a dinuclear complex of $Co^{2+}$ complex has been synthesized. Two different strategies have been designed for synthesizing of the complex, including the hydrothermal method and ultrasonic irradiation. The crystals obtained by the hydrothermal method were structurally characterized by single-crystal X-ray diffraction, while the ultrasonic complex, was obtained as a precipitate. Acceptable matches were observed between powder X-ray diffraction patterns, FT-IR spectra and thermal behavior of the synthesized complexes. This confirmed that the complex which synthesized by a sonochemical process has an identical structure to that obtained by a hydrothermal method. The morphology of the complexes shows nano and microstructures for **uc** and **hc**, respectively. Nano-sized particles of $Co_3O_4$ were used as adsorbents for the removal of Pb(II) from aqueous solutions. The maximum adsorption capacity for $Co_3O_4$-**hc** and $Co_3O_4$- **uc** was found to be 135 and 138.3 mg/g, respectively. After five cycles, the synthetic catalysts of $Co_3O_4$- **uc** and $Co_3O_4$- **hc** showed an excellent cycling performance for Pb(II) desorption up to 85.3 and 83.4%, respectively.

**Acknowledgements** The financial support from University of Zabol (Grant No: 9618-39).

## References

1. Hanifehpour Y, Soltani B, Mirtamizdoust B, Khomami B, Joo SW (2016) Thermolysis synthesis of pure phase nano-sized cobalt(II) oxide from novel cobalt(II)-pyrazole discrete nano coordination compound. J Inorg Organomet Polym Mater 26(2):335–343

2. Kavitha T, Haider S, Kamal T, Ul-Islam M (2017) Thermal decomposition of metal complex precursor as route to the synthesis of $Co_3O_4$ nanoparticles: antibacterial activity and mechanism. J Alloys Compd 704:296–302
3. Asadizadeh S, Amirnasr M, Meghdadi S, Tirani FF, Schenk K (2018) Facile synthesis of $Co_3O_4$ nanoparticles from a novel tetranuclear cobalt(III) complex. Application as efficient electrocatalyst for oxygen evolution reaction in alkaline media. Int J Hydrogen Energy 43(10):4922–4931
4. Zhang F, Hao L, Zhang L, Zhang X (2011) Solid-state thermolysis preparation of $Co_3O_4$ nano/micro superstructures from metal–organic framework for supercapacitors. Int J Electrochem Sci 6:2943–2954
5. Khalaji AD, Nikookar M, Fejfarova K, Dusek M (2014) Synthesis of new cobalt(III) Schiff base complex: a new precursor for preparation $Co_3O_4$ nanoparticles via solid-state thermal decomposition. J Mol Struct 1071:6–10
6. Ezz AA, Kamel MM, Saad GR (2019) Synthesis and characterization of nanocarbon having different morphological structures by chemical vapor deposition over Fe–Ni–Co–Mo/MgO catalyst. J Saudi Chem Soc 23(6):666–677
7. Afify HH, Hassan SA, Obaida M, Abouelsayed A (2019) Influence of annealing on the optical properties of monoclinic vanadium oxide $VO_2$ prepared in nanoscale by hydrothermal technique. Physica E 114:113610
8. Li L, Ren J (2006) Rapid preparation of spinel $Co_3O_4$ nanocrystals in aqueous phase by microwave irradiation. Mater Res Bull 41(12):2286–2290
9. Berber M, Bulto V, Kli R, Hahn H (2005) Transparent nanocrystalline ZnO films prepared by spin coating. Scr Mater 53:547–551
10. Choy JH, Jang ES, Won JH, Chung JH, Jang DJ, Kim YW (2003) Soft solution route to directionally grown ZnO nanorod arrays on Si wafer; room-temperature ultraviolet laser. Adv Mater 15:1911–1914
11. Gómez VJ, Santos AJ, Blanco E, Lacroix B, García R, Huffaker DL, Morales FM (2019) Porosity control for plasma-assisted molecular beam epitaxy of GaN nanowires. Cryst Growth Des 19(4):2461–2469
12. dos Santos Depoi F, de Oliveira TC, de Moraes DP, Pozebon D (2012) Preconcentration and determination of As, Cd, Pb and Bi using different sample introduction systems, cloud point extraction and inductively coupled plasma optical emission spectrometry. Anal Methods 4:89–95
13. Jan MR, Shah J, Sadia M, Atta-ul-Haq (2012) Preconcentration and determination of Pb(II) in aqueous samples using functionalized Dowex 1X8. Solvent Extr Ion Exch 30(3):306–319
14. Cañizares P, Martínez F, Jiménez C, Lobato J, Rodrigo MA (2006) Coagulation and electrocoagulation of wastes polluted with dyes. Environ Sci Technol 40(20):6418–6424
15. Ezoddin M, Shemirani F, Abdi Kh, Saghezchi MK, Jamali MR (2010) Application of modified nano-alumina as a solid phase extraction sorbent for the preconcentration of Cd and Pb in water and herbal samples prior to flame atomic absorption spectrometry determination. J Hazard Mater 178:900–905
16. Zhao L, Chen XF, Wang XC, Zhang YJ, Wei W, Sun YH, Antonietti M, Titirici MM (2010) One-step solvothermal synthesis of a carbon@ $TiO_2$ dyade structure effectively promoting visible-light photocatalysis. Adv Mater 22:3317–3321
17. Wawrzkiewicz M, Polska-Adach E, Hubicki Z (2019) Application of titania based adsorbent for removal of acid, reactive and direct dyes from textile effluents. Adsorption 25(3):621–630
18. Sobhanardakani S, Parvizimosaed H, Olyaie E (2013) Heavy metals removal from wastewaters using organic solid waste—rice husk. Environ Sci Pollut Res 20:5265–5271
19. Sumesh E, Bootharaju MS, Pradeep T (2011) A practical silver nanoparticle-based adsorbent for the removal of $Hg^{2+}$ from water. J Hazard Mater 189(1–2):450–457
20. Karri RR, Shams S, Sahu JN (2019) Overview of potential applications of nano-biotechnology in wastewater and effluent treatment. In: Ahsan A (ed) Nanotechnology in water and wastewater treatment. Elsevier, Amsterdam, pp 87–100
21. Ngah WW, Hanafiah MAKM (2008) Removal of heavy metal ions from wastewater by chemically modified plant wastes as adsorbents: a review. Bioresour Technol 99(10):3935–3948
22. Liu JF, Zhao ZS, Jiang JB (2008) Coating $Fe_3O_4$ magnetic nanoparticles with humic acid for high efficient removal of heavy metals in water. Environ Sci Technol 42(18):6949–6954
23. Xin X, Wei Q, Yang J, Yan L, Feng R, Chen G, Li H (2012) Highly efficient removal of heavy metal ions by amine-functionalized mesoporous $Fe_3O_4$ nanoparticles. Chem Eng J 184:132–140
24. Uddin MK, Baig U (2019) Synthesis of $Co_3O_4$ nanoparticles and their performance towards methyl orange dye removal: characterisation, adsorption and response surface methodology. J Clean Prod 211:1141–1153
25. Yavuz E, Tokalıoğlu S, Şahan H, Patat S (2013) A graphene/$Co_3O_4$ nanocomposite as a new adsorbent for solid phase extraction of Pb(II), Cu(II) and Fe(III) ions in various samples. RSC Adv 3(46):24650–24657
26. Grillo F, Natile MM, Glisenti A (2004) Low temperature oxidation of carbon monoxide: the influence of water and oxygen on the reactivity of a $Co_3O_4$ powder surface. Appl Catal B 48(4):267–274
27. Liu X, Qiu G, Li X (2005) Shape-controlled synthesis and properties of uniform spinel cobalt oxide nanocubes. Nanothechnology 16:3035
28. Wang WW, Zhu YJ (2005) Stimuli-responsive materials for self-healing in corrosion protection. Mater Res Bull 40:1929
29. Hu L, Zhang G, Liu M, Wang Q, Dong S, Wang P (2019) Application of nickel foam-supported $Co_3O_4$–$Bi_2O_3$ as a heterogeneous catalyst for BPA removal by peroxymonosulfate activation. Sci Total Environ 647:352–361
30. Zhao J, Tang Z, Dong F, Zhang J (2019) Controlled porous hollow $Co_3O_4$ polyhedral nanocages derived from metal–organic frameworks (MOFs) for toluene catalytic oxidation. Mol Catal 463:77–86
31. Anke S, Bendt G, Sinev I, Hajiyani H, Antoni H, Zegkinoglou I, Muhler M (2019) Selective 2-propanol oxidation over unsupported $Co_3O_4$ spinel nanoparticles: mechanistic insights into aerobic oxidation of alcohols. ACS Catal 9(7):5974–5985
32. Lou XW, Deng D, Lee JY, Feng J, Archer LA (2008) Self-supported formation of needlelike $Co_3O_4$ nanotubes and their application as lithium-ion battery electrodes. Adv Mater 20:258–262
33. Li WY, Xu LN, Chen J (2005) $Co_3O_4$ nanomaterials in lithium-ion batteries and gas sensors. Adv Funct Mater 15(5):851–857
34. Li LL, ChuY LiuY, Song JL, Wang D, Du XW (2008) A facile hydrothermal route to synthesize novel $Co_3O_4$ nanoplates. Mater Lett 62:1507–1510
35. Meher SK, Rao GR (2011) Ultralayered $Co_3O_4$ for high-performance supercapacitor applications. J Phys Chem C 115:15646–15654
36. Saheli S, Rezvani AR, Malekzadeh A, Dusek M, Eigner V (2018) Novel inorganic precursors $[Co_{4.32}Zn_{1.68}(HCO_2)_{18}(C_2H_8N)_6]/SiO_2$ and $[Co_{4.32}Zn_{1.68}(HCO_2)_{18}(C_2H_8N)_6]/Al_2O_3$ for Fischer–Tropsch synthesis. Int J Hydrogen Energy 43(2):685–694
37. Razmara Z, Rezvani AR, Saravani H (2017) Fischer–Tropsch reaction over a $Co_2$–NiMn/$SiO_2$ nanocatalyst prepared by thermal decomposition of a new precursor. Chem Pap 71(4):849–856
38. Janani H, Rezvani AR, Grivani GH, Mirzaei AA (2016) Preparation and characterization of a new cobalt hydrazone complex and its catalytic activity in the hydrogenation of carbon monoxide (Fischer–Tropsch synthesis). React Kinet Mech Catal 117(1):189–203

39. Saheli S, Rezvani AR, Malekzadeh A, Dusek M, Eigner V (2018) Effect of synthetic route and metal oxide promoter on cobalt-based catalysts for Fischer–Tropsch synthesis. Catal Lett 148(11):3557–3569
40. Razmara Z, Rezvani AR, Saravani H (2018) Molecular structure of inorganic supramolecular compounds and its application as a precursor in producing hydrocarbons. J Mol Struct 1171:503–510
41. Palatinus L, van der Lee A (2008) Symmetry determination following structure solution in P1. J Appl Crystallogr 41:975–984
42. PetricekV Dusek M, Palatinu LZ (2014) Crystallographic computing system JANA2006: general features. Z Kristallogr Cryst Mater 229:345–352
43. Nathan LC, Mai TD (2000) Influence of the spectator cation on the structure of anionic pyridine-2, 6-dicarboxylato complexes of cobalt(II), nickel(II), and copper(II). J Chem Crystallogr 30(8):509–518
44. Kirillova MV, da Silva MFCG, Kirillov AM, da Silva JJF, Pombeiro AJ (2007) 3D hydrogen bonded heteronuclear $Co^{II}$, $Ni^{II}$, $Cu^{II}$ and $Zn^{II}$ aqua complexes derived from dipicolinic acid. Inorg Chim Acta 360:506
45. Cai M, Chen J, Taha M (2010) Synthesis, structures and antibacterial activities of two complexes of yttrium(III) with 2, 6-pyridinedicarboxylate. Inorg Chem Commun 13:199–202
46. Mohandes F, Davar F, Salavati-Niasari M (2010) Preparation of $Co_3O_4$ nanoparticles by nonhydrolytic thermolysis of [Co (Pht) $(H_2O)]_n$ polymers. J Magn Magn Mater 322(7):872–877
47. Akhbari K, Morsali A (2008) Thermal, solution and structural studies of a 3D Ag(I) coordination polymer with various Ag–Ag bonds,$[Ag_3$ (μ-Hbtc)(μ-$H_2$btc)$]_n$. J Iran Chem Soc 5:48–56
48. Saheli S, Rezvani A (2017) A novel coordination polymer of Ni(II) based on 1, 3, 5-benzenetricarboxylic acid synthesis, characterization, crystal structure, thermal study, and luminescent properties. J Mol Struct 1127:583–589
49. Marandi F, Ghorbanloo M, Soudi AA (2007) Lead(II) complexes of o-phthalate including a crystal structure of a novel 2D coordination polymer,[Pb (pht)(H2O)]$_n$. J Coord Chem 60:1557–1565
50. Saheli S, Rezvani AR, Rigi S, Dusek M, Eigner V, Jarosova M (2019) Design of mixed metal oxides with increased catalytic activity for Fischer–Tropsch synthesis. Catal Lett 149(12):3257–3267
51. Pugazhenthiran N, Sathishkumar P, Murugesan S, Anandan S (2011) Effective degradation of acid orange 10 by catalytic ozonation in the presence of Au–$Bi_2O_3$ nanoparticles. Chem Eng J 168(3):1227–1233
52. Hayati P, Rezvani AR, Morsali A, Retailleau P, García-Granda S (2017) Influences of temperature, power ultrasound and reaction time on the morphological properties of two new mercury(II) coordination supramolecular compounds. Ultrason Sonochem 34:968–977
53. Herrero NM, Benito P, Labajos FM, Rives V (2007) Nanosize cobalt oxide-containing catalysts obtained through microwave-assisted methods. Catal Today 128:129–137
54. Tuti S, Pepe F (2008) On the catalytic activity of cobalt oxide for the steam reforming of ethanol. Catal Lett 122(1–2):196–203
55. Sharma N, Jha R, Baghel S, Sharma D (2017) Study on photocatalyst zinc oxide annealed at different temperatures for photodegradation of Eosin Y dye. J Alloys Compd 695:270–279
56. Klug PH, Alexander LE (1974) X-ray diffraction procedures. Wiley, New York
57. Deraz NAM (2002) Catalytic decomposition of $H_2O_2$ on promoted cobaltic oxide catalysts. Mater Lett 57:914–920
58. Azali NS, Kamarudin NHN, Rahim ARA, Nasir NSAJ, Timmiati SN, Jaafar NF (2019) Adsorption and release of 5-fluorouracil (5FU) from mesoporous silica nanoparticles. Mater Today Proc 19:1722–1729
59. Abdolmohammad-Zadeh H, Ayazi Z, Hosseinzadeh S (2019) Application of $Co_3O_4$ nanoparticles as an efficient nano-sorbent for solid-phase extraction of zinc(II) ions. Microchem J 153:104268
60. Bagheri H, Afkhami A, Saber-Tehrani M, Khoshsafar H (2012) Preparation and characterization of magnetic nanocomposite of Schiff base/silica/magnetite as a preconcentration phase for the trace determination of heavy metal ions in water, food and biological samples using atomic absorption spectrometry. Talanta 97:87–95
61. Karatapanis AE, Petrakis DE, Stalikas CD (2012) A layered magnetic iron/iron oxide nanoscavenger for the analytical enrichment of ng-$L^{-1}$ concentration levels of heavy metals from water. Anal Chim Acta 726:22–27
62. Yavuz E, Tokalıoğlu S, Şahan H, Patat S (2013) Ultralayered $Co_3O_4$ as a new adsorbent for preconcentration of Pb(II) from water, food, sediment and tobacco samples. Talanta 115:724–729
63. Talebzadeh F, Zandipak R, Sobhanardakani S (2016) $CeO_2$ nanoparticles supported on $CuFe_2O_4$ nanofibers as novel adsorbent for removal of Pb(II), Ni(II), and V(V) ions from petrochemical wastewater. Desalin Water Treat 57(58):28363–28377
64. Munagapati VS, Wen JC, Pan CL, Gutha Y, Wen JH (2019) Enhanced adsorption performance of Reactive Red 120 azo dye from aqueous solution using quaternary amine modified orange peel powder. J Mol Liq 285:375–385
65. Emerson H, Kaplan DI, Powell BA (2019) Plutonium binding affinity to sediments increases with contact time. Chem Geol 505:100–107
66. Yakout AA, Shaker MA, Elwakeel KZ, Alshitari W (2019) Lauryl sulfate@ magnetic graphene oxide nanosorbent for fast methylene blue recovery from aqueous solutions. J Disper Sci Technol 40(5):707–715
67. Senthilkumaar S, Varadarajan PR, Porkodi K, Subbhuraam CV (2005) Adsorption of methylene blue onto jute fiber carbon: kinetics and equilibrium studies. J Colloid Interface Sci 284(1):78–82
68. Khan SB, Rahman MM, Asiri AM, Marwani HM, Bawaked SM, Alamry KA (2013) $Co_3O_4$ co-doped $TiO_2$ nanoparticles as a selective marker of lead in aqueous solution. New J Chem 37(9):2888–2893
69. ZhuY HuJ, Wang J (2012) Competitive adsorption of Pb(II), Cu(II) and Zn(II) onto xanthate-modified magnetic chitosan. J Hazard Mater 221:155–161
70. Bhattacharyya KG, Sharma A (2004) Adsorption of Pb(II) from aqueous solution by *Azadirachta indica* (Neem) leaf powder. J Hazard Mater 113(1–3):97–109
71. Hao L, Song H, Zhang L, Wan X, Tang Y, Lv Y (2012) $SiO_2$/graphene composite for highly selective adsorption of Pb(II) ion. J Colloid Interface Sci 369(1):381–387
72. Deng X, Li Lü, Li H, Luo F (2010) The adsorption properties of Pb(II) and Cd(II) on functionalized graphene prepared by electrolysis method. J Hazard Mater 183(1–3):923–930
73. Madadrang CJ, Kim HY, Gao G, Wang N, Zhu J, Feng H, Hou S (2012) Adsorption behavior of EDTA-graphene oxide for Pb(II) removal. ACS Appl Mater Int 4(3):1186–1193
74. Koopal L, Tan W, Avena M (2019) Mixed ad/desorption kinetics unraveled with the equilibrium adsorption isotherm. Colloids Surf A Physicochem Eng Asp 577:709–722
75. Zou L, Shao P, Zhang K, Yang L, You D, Shi H, Luo X (2019) Tannic acid-based adsorbent with superior selectivity for lead(II) capture: adsorption site and selective mechanism. Chem Eng J 364:160–166
76. Wang N, Qiu Y, Xiao T, Wang J, Chen Y, Xu X, Yu H (2019) Comparative studies on Pb(II) biosorption with three spongy microbe-based biosorbents: high performance, selectivity and application. J Hazard Mater 373:39–49